Ionic liquid diffusion properties in tetrapod-like ZnO photoanode for dye-sensitized solar cells

Kun-Mu Lee [a,b,*], Wei-Hao Chiu [b], Chih-Yu Hsu [c], Hsin-Ming Cheng [d], Chia-Hua Lee [e], Chun-Guey Wu [b]

[a] Department of Chemical and Materials Engineering, National Central University, Taoyuan 32001, Taiwan
[b] Research Center for New Generation Photovolatics, National Central University, Taoyuan 32001, Taiwan
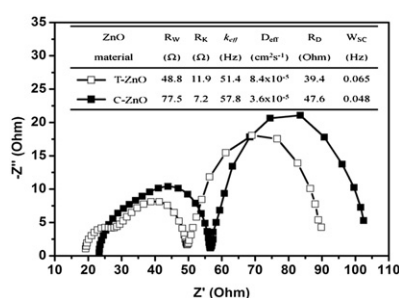[c] Institute of Chemistry, Academia Sinica, Taipei 11529, Taiwan
[d] Research Center for Applied Sciences, Academia Sinica, Taipei 11529, Taiwan
[e] Department of Materials Science and Engineering, National Tsing-Hua University, Hsinchu 30013, Taiwan

HIGHLIGHTS

► The tetrapod-like ZnO nanopowder provides fast electron transport in ZnO and efficient ionic diffusion pathway in the photoanode pore.
► The recombination rate of T-ZnO-based DSC is lower than that of C-ZnO one.
► The ion diffusion ability in tetrapod-like ZnO is about two times improvement, which enables the regeneration ability of dye molecular by redox couples.

GRAPHICAL ABSTRACT

ZnO material	R_W (Ω)	R_K (Ω)	k_{eff} (Hz)	D_{eff} (cm²s⁻¹)	R_D (Ohm)	W_{SC} (Hz)
T-ZnO	48.8	11.9	51.4	8.4×10^{-5}	39.4	0.065
C-ZnO	77.5	7.2	57.8	3.6×10^{-5}	47.6	0.048

ARTICLE INFO

ABSTRACT

Dye-sensitized solar cells (DSCs) are a promising PV device to solve global energy-related problems because it is clean, inexhaustible and readily available. In order to improve the stability and reliability of the DSCs, ionic liquid (IL) electrolyte is a good choice for replacement of volatile solvent electrolyte systems (e.g. acetonitrile). However, the high viscosity of ionic liquids leads to mass-transport limitations on the photocurrents in the DSCs. In this report, a new porous photoanode made by tetrapod-like ZnO (T-ZnO) nanopowders provides not only a fast electron transport path in ZnO but also an efficient ionic diffusion pathway in the photoanode pore, comparing to the spherical commercial ZnO (C-ZnO) nanopowders. In addition, the ionic diffusion dynamics of T-ZnO and C-ZnO devices are characterized by electrochemical impedance analysis (EIS), photocurrent transient dynamics. We observed the presence of a tetrapod-like framework, which allowed the photoanode to provide a more efficient ionic diffusion pathway than conventional one made of commercial spherical nanopowders provided.

© 2012 Elsevier B.V. All rights reserved.

1. Introduction

The past decade has seen much research into dye-sensitized solar cells (DSCs) and more than a thousand journal articles describe this vibrant area of research. DSCs have low angle dependency on incident light and operate at high efficiency. These devices have low manufacturing costs and are considered environmentally friendly [1–3]. A DSC is fabricated from several

* Corresponding author. Department of Chemical and Materials Engineering, National Central University, Taoyuan 32001, Taiwan. Tel.: +886 3 5913135; fax: +886 3 5820206.
E-mail address: kmlee@ncu.edu.tw (K.-M. Lee).

components: a counter electrode, electrolyte, and a nonporous photoanode with anchoring a dye absorber that harvest the sunlight and inject the excited electron into the photoanode. The redox-active species, commonly I_3^-/I^- redox couples, in the electrolytes regenerate the excited dye on the photoanode in order to re-absorb photon and exchange current density corresponding to the electrocatalytic activity at the counter electrode. Therefore, the efficient redox ionic diffusion is a prerequisite for an efficient DSC due to fast light re-absorption by dye regeneration.

C.G. Wu, and M. Grätzel et al. [4] reported the ruthenium-sensitized solar cell devices had achieved better than 11.5% power conversion efficiency using a TiO$_2$ porous film. The volatile solvent electrolytes used in the high performance DSCs have good ionic diffusion ability and low boiling point that reduce the stability of the device. In order to solve this important issue in view of the practical application, nonvolatile viscous ionic liquid electrolytes, quasi-solid state electrolytes, and solid state electrolytes have been introduced to replace for the volatile solvent electrolytes. However, the ionic diffusion of these viscous electrolytes in the nano-crystalline network structure limits the device performance. In order to improve the ionic diffusion ability for the viscous or quasi-solid-state electrolytes, additives are used in the electrolyte, such as nanosilicate platelets [5] or SiO$_2$ nanoparticles [6]. Moreover, D. Zhu et al. successfully demonstrated an electrohydrodynamic (EHD) technique to prepare TiO$_2$ photoanodes with hierarchical branched inner channels, and efficiently improved the transport properties of redox-active species in viscous electrolytes [7].

In order to fabricate photoanode with hierarchical structure, ZnO is an excellent candidate. ZnO has similar band gap and conduction band energy level to TiO$_2$ but offers good electron mobility. ZnO has been widely fabricated into 0D and 1D nano-structures, including pop-corn style DSCs [8,9], nanowires (NWs) [10], branched NWs [11], and tetrapod particles [12–14] for DSCs application.

In this work, we report the use of tetrapod-like ZnO (T-ZnO) nanopowder to form a porous framework for efficient electron transport in the photoanode, and to provide improved ionic diffusion electrolyte within the photoanode pore, comparing to the spherical commercial ZnO (C-ZnO) nanopowder. We also analyzed and discussed these performances, referring to various experimental measurements, including incident monochromatic photon to current conversion efficiency (IPCE), photocurrent transient dynamics, and electrochemical impedance spectroscopy (EIS).

2. Experimental

2.1. Preparation of tetrapod-like ZnO nanoparticles

A novel 70 kW DC plasma reactor was used to synthesize T-ZnO nanoparticles (NPs) under atmospheric pressure. We used commercially obtained zinc powder (Alfa Aesar) with an average particle size of 10 μm, and with less than 50 ppm of Cr, Fe, and Pb impurity. The zinc powders underwent vaporization, oxidation, and quenching in the plasma flame. The plasma-forming gas was 50% Ar and 50% N$_2$, the carrier gas was N$_2$, and the quenching gas was an Air and N$_2$ mix. The reactor synthesis rate for T-ZnO NPs was in excess of 1 kg h^{-1}. The detailed synthetic procedure was reported previously in references [15,16].

2.2. Device fabrication

The T-ZnO NPs were mixed with ethyl cellulose (EC), and anhydrous terpineol (Fluka) for screen-printing the ZnO paste [17]. We used ZnO nanoparticle (C-ZnO) (Seedchem, Australia) with a specific surface area of 18.03 m^2 g^{-1}, following the same

procedure as for the T-ZnO paste, to provide a comparison with T-ZnO. The two different ZnO pastes were screen-printed to 0.28 cm^2 photoanode electrodes on fluorine-doped tin oxide glass (FTO, Nippon Sheet Glass, 7 Ω square^{-1}, 2.2 mm thick) without a blocking layer, and then heated under an air flow at 400 °C for 60 min. After cooling to room temperature, the ZnO photoanode electrodes were immersed in a D149 organic sensitizer solution (0.5 mM) [18] (Mitsubishi Paper Mills Limited), and 1 mM chenodeoxycholic acid (CDCA, Sigma−Aldrich), in an acetonitrile/tert-butyl alcohol mixture (v/v = 1/1) at 65 °C for 30 min, and the photoanode electrode then rinsed with acetonitrile (AN). The cell was covered with platinized FTO glass incorporating a drilled hole, to form the counter electrode and complete the sandwich configuration. The cell interior was separated by a 30 μm thick Surlyn polymer spacer (Surlyn, Dupont), and filled with electrolyte via the hole in the counter electrode. The acetonitrile-based (AN-based) electrolyte was composed of 1,2-dimethyl-3-propylimidazolium iodide (PMII) (0.6 M), tert-butylpyridine (TBP, Sigma−Aldrich) (0.5 M) in acetonitrile (AN) and I$_2$ (0.05 M). The IL-based electrolyte comprised I$_2$ (0.2 M), and TBP (0.5 M) in a PMII/1-Octy-3-methylimidazolium hexafluorophosphate (C$_8$MImPF$_6$) mixture (v/v = 35/65). Finally, drill holes were sealed using Surlyn hot-melt polymer and cover glasses.

2.3. Characterization

DSC illumination for photovoltaic measurements employed a 100 mW cm^{-2} white light source (Yamashita Denso, YSS-100A), and the light source power output was calibrated using a reference Si photodiode (BS-520, Bunko Keiki). The simulated light spectrum was consistent with class A JISC-8912. The DSC photovoltaic characteristics were obtained by applying an external potential bias to the cell, and measuring the generated photocurrent using an electrochemical analyzer (Autolab, PGSTAT30). The AN-based and IL-based DSC scan rates were 50 mV s^{-1} and 5 mV s^{-1}, respectively. For electrochemical impedance spectroscopy (EIS) measurement, an AM 1.5G white light source was used and illuminated on the surface of the solar cell. The applied bias was set for open-circuit voltage, with AC amplitude of 10 mV, and a scanned frequency range of 1 mHz−1 MHz. To measure the ionic diffusion resistance in ZnO films, the C-ZnO and T-ZnO films were tested in the AN solution, which containing 5 mM LiI and 0.5 mM I$_2$, by applying voltage of −0.5 V (vs. Ag/Ag$^+$) in a typically electrochemical three-electrode system (ZnO film, Pt plate and Ag/Ag$^+$ as working electrode, counter electrode and reference electrode, respectively). Photocurrent action spectra for the incident monochromatic photon to current conversion efficiency (IPCE) were taken with an IPCE measurement system (C-995, PV-measurement Inc.). The morphologies and dimensions of ZnO films were characterized using a JEOL-6500 field emission scanning electron microscope (FE-SEM) operating at 10 keV. The surface area was determined by the Micrometrics ASAP (Accelerated Surface Area and Porosimetry) System 2010.

3. Results and discussion

3.1. Morphology of ZnO photoanode and photovoltaic performance

Photoanode morphology plays an important role in dye-sensitized solar cells, especially for high viscosity or quasi-solid state electrolyte. The electrolyte fills the pore of photoanode determines diffusion rates of the I_3^-/I^- redox couple. Fig. 1(a) and (b) shows cross-sectional FE-SEM images of C-ZnO and T-ZnO films on FTO glass, and Fig. 1(c) and (d) are the zoom-in images. Each of the 26 μm thick photoanodes exhibit highly porous nanostructures, the
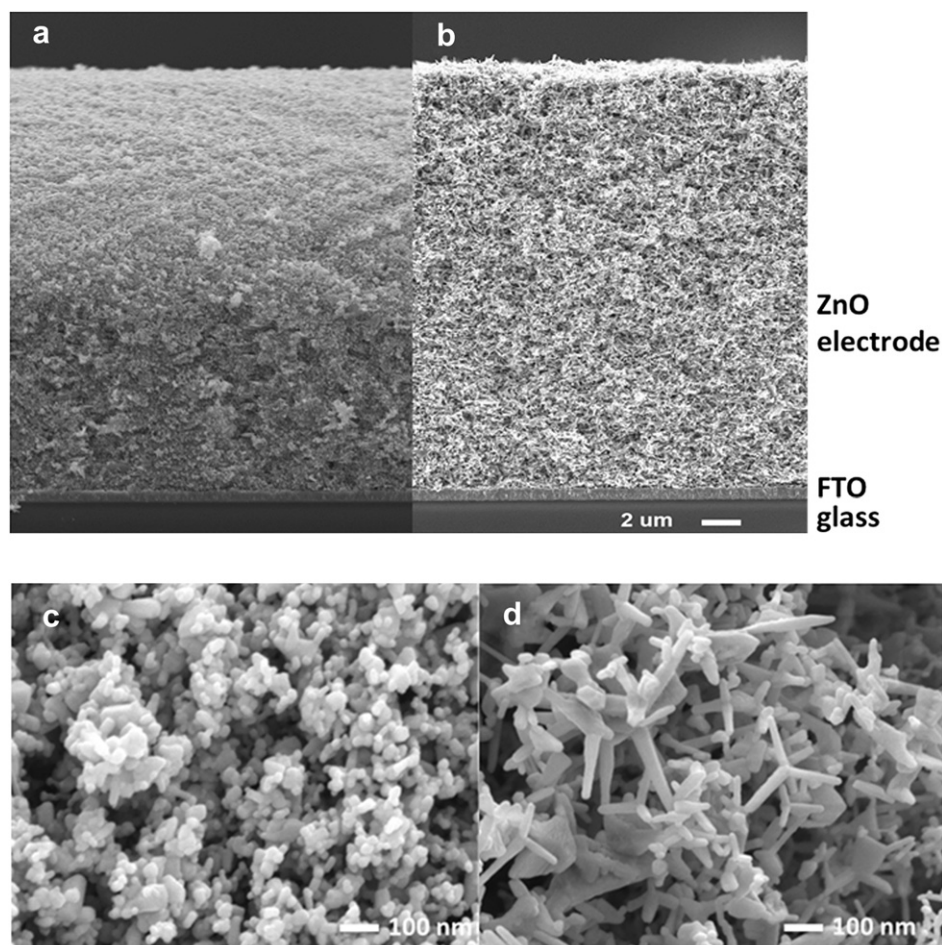
Fig. 1. The side view of SEM images of (a) C-ZnO and (b) T-ZnO electrode, and (c) and (d) are the zoom-in image, respectively.

C-ZnO and T-ZnO film surface areas are approximately 18.03 $m^2\,g^{-1}$ and 15.72 $m^2\,g^{-1}$, respectively. The porous network provided by the T-ZnO film provides both an efficient photoanode electron diffusion path [13,14], and larger pore size than the C-ZnO nanopowder film, due to the tetrapod-like morphology. As showed in Table 1, the amount of dye adsorbed are 3.93×10^{-8} and 3.82×10^{-8} mol cm^{-2} for C-ZnO and T-ZnO electrode, respectively. With AN-based electrolyte, the values of J_{SC} are 10.95 and 11.60 mA cm^{-2}, and values of V_{OC} are 0.615 and 0.630 V for that with C-ZnO and T-ZnO electrode, respectively. It is due to T-ZnO electrode has lower electron transport resistance and higher electron lifetime. However, in IL-based DSC, the values of J_{SC} are 3.75 and 5.00 mA cm^{-2} for that with C-ZnO and T-ZnO electrode, due to the ion-transport resistance.

For comparison, the T-ZnO photoanode thicknesses were varied from 6 to 26 μm. Fig. 2 shows photovoltaic characteristics under one sun illumination, for AN-based and IL-based electrolytes. Fig. 2(a) provides the open-circuit voltage (V_{OC}) results for DSCs

using each electrolyte and the V_{OC} decreases linearly with the increase of ZnO film thickness for both electrolytes. Inhomogeneous light intensity in the porous ZnO films contributes to a photoanode inhomogeneous quasi-Fermi level. We attributed a 200 mV V_{OC} reduction, in IL-based DSCs, relative to the AN-based DSCs with the same thickness in ZnO film, as due to the higher I_2 concentration in IL-based DSCs. This effect is explained by charge recombination between the photoanode and I_3^-/I^- couples in the electrolyte as given by the following equation [19]:

$$V_{OC} = \left[\frac{kT}{e}\right] \ln \left[\frac{I_{inj}}{n_{cb} k_{et} \left[I_3^-\right]}\right]$$

where k is the Boltzmann constant, T is the absolute temperature, e is the electronic elementary charge, I_{inj} is the sensitized dye charge flux, n_{cb} is the electron concentration within ZnO, k_{et} is the reaction rate constant for the dark current from ZnO to tri-iodide ion in the electrolyte, and $[I_3^-]$ is the tri-iodide ion concentration in the electrolyte. Fig. 2(b) shows the variation in short-circuit photocurrent (J_{SC}) with film thickness. J_{SC} for AN-based DSCs increases continuously with film thickness, reaching a maximum value of 11.4 mA cm^{-2} at a thickness of 26 μm. By contrast, J_{SC} values of IL-based DSC plateau close to 5 mA cm^{-2} in devices with around 18 μm thickness. The FF remains constant for the AN-based DSCs, while the IL-based DSCs exhibit a prominent decline in FF with increasing film thickness. These different J_{SC} and FF behaviors result from higher viscosity of ionic liquid, which limit mass-transport of

Table 1
The photovoltaic performance and properties of AN-based DSC with C-ZnO and T-ZnO electrodes, respectively, under 100 mW cm^{-2} (AM 1.5).

Electrode	Amount of dye adsorption (mol cm^{-2})	J_{SC} (mA cm^{-2})	V_{OC} (V)	FF	Eff. (%)	τ_e (ms)[a]
C-ZnO	3.93×10^{-8}	10.95	0.615	0.62	4.14	21.5
T-ZnO	3.82×10^{-8}	11.60	0.630	0.64	4.68	23.2

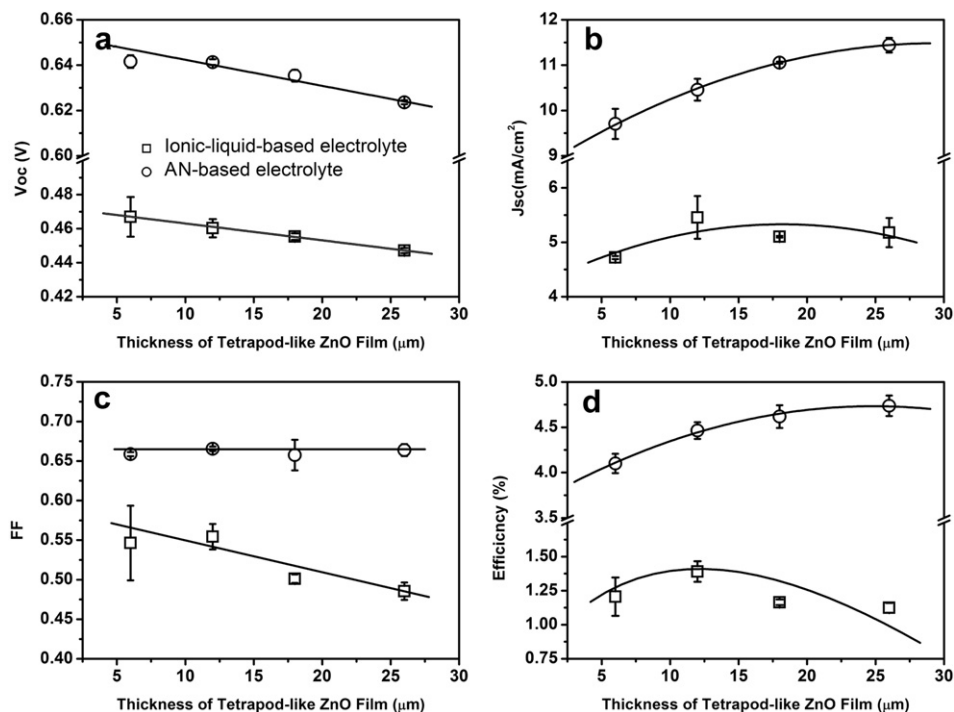[a] τ_e: electron lifetime, calculated from EIS fitting data.

Fig. 2. Dependences of cell performances on film thickness, including (a) open-circuit voltage (V_{OC}), (b) short-circuit photocurrent density (J_{SC}), (c) filling factor (*FF*), and (d) solar conversion efficiency. All data are obtained under one sun irradiation. The open-circle and open-square symbols correspond to DSCs with AN-based and IL-based electrolytes, respectively. The lines are plotted to guide the eyes, and the error bars from the data of the two devices are shown.

I_3^-/I^- couples in the electrolyte, and increase ions diffusion resistance. The maximal conversion efficiencies obtained for both AN and IL-based DSCs, as calculated by the relation $\eta = J_{SC} \times V_{OC} \times FF$ at one sun irradiation, are 4.73% for 26 μm thick T-ZnO electrode, and 1.39% for 12 μm thick electrode, respectively. Therefore, for IL-based DSCs, the thickness of photoanode is not a major factor for device optimization as competing with ionic liquid characteristics or the morphology of photoanode.

Fig. 3(a) shows *J*−*V* curves of DSC devices fabricated using the T-ZnO photoanode and the one made of spherical C-ZnO NPs, respectively. The photovoltaic parameters of AN-based DSCs with 26 μm T-ZnO photoanode are $V_{OC} = 0.622$ V, $J_{SC} = 11.55$ mA cm^{-2}, $FF = 0.67$ and $\eta = 4.81\%$. IL-based DSCs however produce lower performances, in which the photovoltaic parameters of 26 μm T-ZnO-based DSCs are $V_{OC} = 0.448$ V, $J_{SC} = 5.37$ mA cm^{-2}, $FF = 0.48$, and $\eta = 1.15\%$. Those of 26 μm C-ZnO-based DSCs are $V_{OC} = 0.444$ V, $J_{SC} = 3.95$ mA cm^{-2}, $FF = 0.49$, and $\eta = 0.87\%$. A high photocurrent of 11.55 mA cm^{-2} is achieved with high absorption coefficient of D149 in AN-based electrolyte system, while a half-less photocurrent was obtained in IL-based system. The viscosity limits the ionic transport in the IL-based electrolyte, which in turn limits the photocurrent. Once T-ZnO photoanode is employed, the IL-based DSC produces photocurrent with *ca.* 1.3 times larger than that for a C-ZnO photoanode, owing to the larger pore size in the tetrapod framework, which provides an efficient ionic diffusion pathway and thus improves the ionic-transport capacity. We used IPCE spectroscopy to determine the photon to photocurrent conversion efficiency for incident wavelength-dependent photon. The IPCE spectra in Fig. 3(b) shows that T-ZnO DSCs containing AN-based electrolyte produce high IPCE values; peak values occur at about 550 nm and 390 nm that attributes the absorption of D149 dye and ZnO, respectively. Although D149 exhibits a strong green light extinction coefficient (68,700 mol^{-1} cm^{-1} at 526 nm), the IPCE spectrum for T-ZnO DSCs containing IL-based electrolyte shows
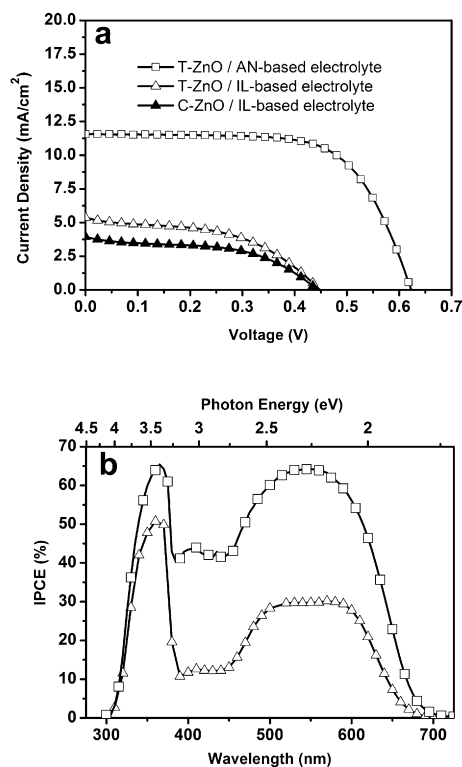

Fig. 3. Cell performances of AN-based (square symbol) and IL-based (triangle symbol) DSCs, based on 26 μm-thick ZnO photoanodes constructed from commercial ZnO (solid symbol, C-ZnO), and tetrapod-like ZnO (open symbol, T-ZnO) nanopowders. (a) The *J*−*V* curve for these DSC devices (100 mW cm^{-2}, AM 1.5G), and (b) the IPCE spectra for these DSC devices.

a plateau between 500 nm and 600 nm at about 30% of the expected D149 absorption. Since worse ionic diffusion in viscous ionic liquid electrolyte slows the regeneration rate of dye molecule. Furthermore, difference across the entire range of the IPCE spectrum is also observed. There is almost 4-fold intensity difference in IPCE band from 400 nm to 450 nm between the two electrolyte devices, due to greater light absorption in the IL-based device from the higher iodine concentration [20]. The observed J_{SC} value is in agreement with the value obtained by integration of the IPCE spectrum under one sun (AM 1.5G). As a result, IPCE illustrates the difference contributions in J_{SC} for DSCs between AN-based and IL-based electrolytes.

3.2. Ionic electrolyte dynamics in ZnO DSCs

In order to understand the ionic-transport mechanism, we carried out time-response photocurrent transients measurements. Fig. 4(a) shows a plot of the time-response short-circuit photocurrent for 12 μm thick tetrapod-ZnO-based DSCs containing IL-based electrolyte, and fitted with an on-off irradiation shutter. Measurements are taken at various sunlight intensities. When commencing to open the shutter, a higher photocurrent is obtained because of a high I^- ion concentration. Subsequently, the

concentration of I^- surrounding dye molecules diminishes due to slow mass transfer of the I_3^-/I^- couples, hence the photocurrent decreases continuously over a few seconds. Finally, the photocurrent reaches steady, depending on the ionic diffusion ability of the ionic liquid electrolyte. As light intensity is reduced, the decreased variation in photocurrents also reduces due to less I^- ions are required to regenerate excited dye molecules. Even in the viscous ionic liquid electrolyte with hindered ionic diffusion, the diffusion of I_3^-/I^- ions to and from the counter electrode provides sufficient redox agents that regenerate the excited dye molecules. Fig. 4(b) shows the ratio of the final and initial photocurrents as functions of film thickness, and light intensity. For IL-based DSCs with a T-ZnO photoanode, the reduction ratio of the photocurrent increases with film thickness and light intensity. Thicker photoanode is able to provide longer effective ionic-transport pathways, so the role of ionic diffusion is more important. Moreover, a comparison of DSCs using 26 μm thick T-ZnO and C-ZnO photoanodes shows that efficient ion-transport pathways within T-ZnO self-assembled photoanode do improve ionic diffusion leading to larger short-circuit photocurrent (Fig. 3(a)).

3.3. Electrochemical impedance spectroscopy analysis

Electrochemical impedance spectroscopy (EIS) is powerful in determining interfacial characteristics of each component in DSC device, and here we focus on photoanode and electrolyte. Fig. 5(a) shows an equivalent electric circuit model [14,21], in which R_W is the electron transport resistance inside the ZnO photoanode. R_K is the charge transfer resistance related to recombination of electrons. R_{FZ} is the resistance at the FTO/ZnO interface, and R_{FTO} is the resistance at the FTO/electrolyte interface. R_{Pt} is the resistance at the Pt surface, and R_S represents the transport resistance of FTO and external circuits. C_μ is the chemical capacitance of the ZnO electrode; C_{FZ}, C_{FTO}, and C_{Pt} represent the constant phase element (equivalent electrical circuit component modeling the behavior of a double layer, an imperfect capacitor) for each corresponding component. Z_N symbolizes the Warburg diffusion impedance, described by the following equation [22],

$$Z_N = \frac{R_D}{\sqrt{j\omega/W_{sc}}}\tanh\left[\sqrt{j\omega/W_{sc}}\right],$$

where R_D is the dc resistance of impedance for tri-iodide diffusion, $W_{sc} = D \times d^{-2}$, where d is the Nernst diffusion layer thickness, and D is the diffusion coefficient for I_3^- ion. Fig. 5(b) shows the Nyquist plots of the IL-based DSC devices with C-ZnO and T-ZnO photoanodes, respectively, under one sun irradiation (AM 1.5G). The inset table shows the corresponding fitting EIS parameters. The R_D values of C-ZnO- and T-ZnO-based devices are 47.6 and 39.4 Ω, respectively. This suggests that for T-ZnO device, the redox carrier diffusion is more efficient than that for C-ZnO one. The effective rate constant for recombination (k_{eff}) characterizes the recombination rate of electrons in the photoanode and I_3^- ions in the electrolyte, i.e. the so-called back-recombination rate. It is clear that the recombination rate of T-ZnO device is lower than that of the C-ZnO one. On the other hand, the recombination resistance (R_K) of T-ZnO device is larger with respect to the C-ZnO one. It is convinced that the efficient ionic diffusion of T-ZnO device causes lower I_3^- concentration around the dye molecular related to the C-ZnO one. Furthermore, the electron diffusion resistance in the photoanode (R_W) of T-ZnO device is smaller than that of the C-ZnO one, due to good electron transport ability of ZnO tetrapod network. Consequently, the better effective electron diffusion coefficient in T-ZnO device gives higher photovoltaic performances, which is consistence to Fig. 3(a).
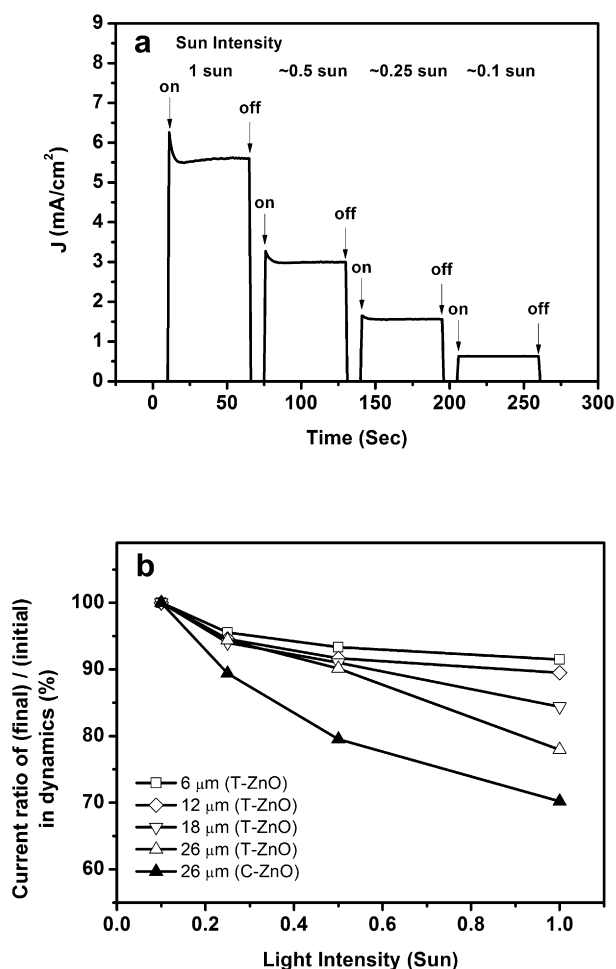
Fig. 4. (a) Photocurrent dynamics obtained with the IL-based DSC device for 12 μm-thick tetrapod-like ZnO (T-ZnO) photoanode. Inset numbers represent the illumination power. (b) Ratio of final to initial photocurrent value as a function of light intensity for different photoanodes. The open and solid symbol represent the photoanodes using tetrapod-like ZnO (T-ZnO) and commercial ZnO (C-ZnO) nanopowders, respectively.
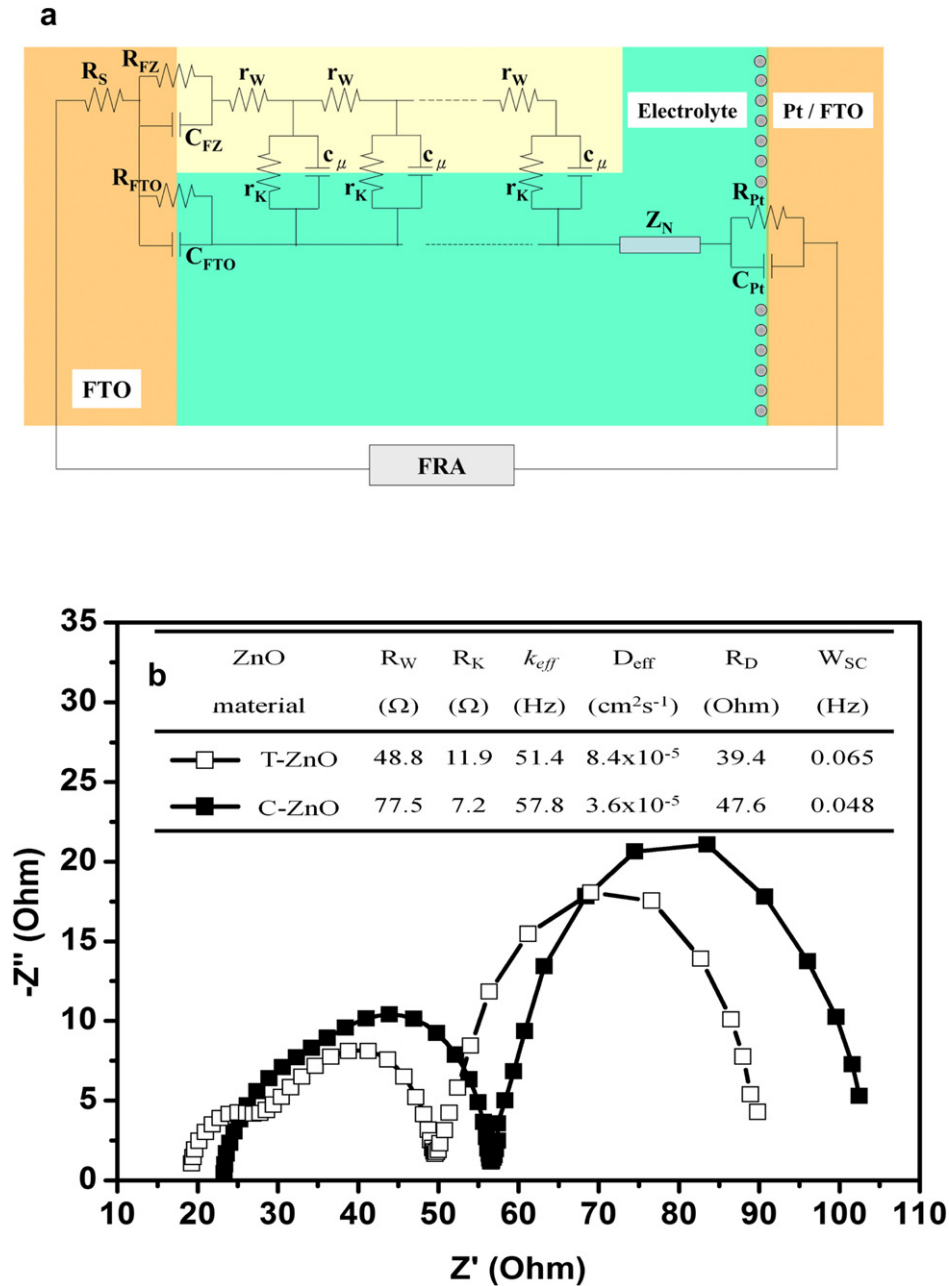
Fig. 5. Electrical characteristics of the IL-based D149-sensitized solar cells. (a) The equivalent circuit model used to analyze experimental data. (b) Nyquist plots for DSCs employing 26 μm commercial ZnO (C-ZnO) and tetrapod-like ZnO (T-ZnO) photoanode. The inset table shows the corresponding fitting parameters.

We further investigate the ionic diffusion behavior within the C-ZnO and T-ZnO films by EIS characterization as shown in Fig. 6(a). The high frequency range could be assigned to the charge transfer reaction, and the response in the low frequency range addresses the ionic diffusion in ZnO film. Thus, the diffusion coefficients of I_3^- ion ($D_{I_3^-}$) within the two ZnO films are obtained by fitting the data at the low frequency rage, i.e. Warburg region, with the following equation [23]:

$$D_{I_3^-} = \frac{R^2 T^2}{2A^2 n^4 F^4 \sigma^2 C_{I_3^-}^2}$$

where A is area of the electrode, $C_{I_3^-}$ is bulk concentration of I_3^- ion and σ is the Warburg factor that is related to Z_{RE}:

$$Z_{RE} = R_S + R_{ct} + \sigma \omega^{-1/2}$$

where Z_{RE}, R_S and R_{ct} are the real part of impedance, solution resistance and charge transfer resistance, respectively. The other symbols have their usual electrochemical meanings. The σ values are obtained from the slopes of linear fitting lines in Fig. 6(b), which are 2390 and 1506 for C-ZnO and T-ZnO, respectively. Thus, the values of $D_{I_3^-}$ are consequently calculated as 1.94×10^{-8} cm² s⁻¹ for C-ZnO film and 4.88×10^{-8} cm² s⁻¹ for T-ZnO film, respectively. Accordingly, the ion diffusion ability in tetrapod-like structure is about two times improvement, which enables the regeneration ability of dye molecular by redox couples as reflecting in the photocurrent increase. It is noted that the diffusion coefficients of I_3^- ion within ZnO films in the order of 10^{-8} cm² s⁻¹ are relative low comparing with that in the bulk solution [24]. Except the viscous
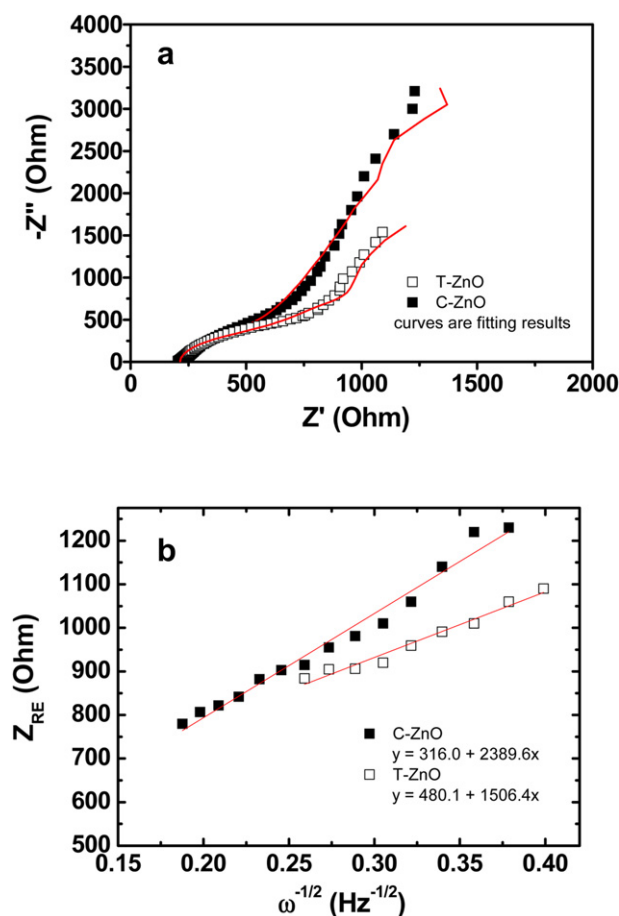
Fig. 6. EIS analysis of C-ZnO and T-ZnO electrodes as working, Pt plate as counter, and Ag/Ag⁺ as reference electrodes in IL-based electrolyte with the frequency ranging from 20,000 to 1 Hz and amplitude of 10 mV. (a) Nyquist plots. (b) The real Z-value as a function of angular frequency at low frequency rage.

nature of IL electrolyte, the ZnO framework also limits the diffusing ability. Therefore, the performance of the ZnO DSCs should be able to further improve by ZnO structure design.

4. Conclusion

In summary, we reported that the length of the ionic diffusion pathway within photoanodes indeed influences photovoltaic performances of IL-based DSCs. With utilizing time-response photocurrent transient measurements and EIS analysis, we have demonstrated that the DSCs with a tetrapod-like framework photoanode deliver enhanced solar-conversion efficiency and short-circuit photocurrents instead of using commercially available sphere powders. Since tetrapod-like structure provides efficient ionic diffusion pathways. Tetrapod-like ZnO is a suitable material for solvent-free DSCs for its efficient electron diffusion and ionic diffusion in the photoanode.

References

[1] J.M. Kroon, N.J. Bakker, H.J.P. Smit, P. Liska, K.R. Thampi, P. Wang, S.M. Zakeeruddin, M. Gratzel, A. Hinsch, S. Hore, U. Wurfel, R. Sastrawan, J.R. Durrant, E. Palomares, H. Pettersson, T. Gruszecki, J. Walter, K. Skupien, G.E. Tulloch, Progress in Photovoltaics 15 (2007) 1–18.
[2] M. Grätzel, Nature 414 (2001) 338–344.
[3] M. Grätzel, Progress in Photovoltaics 8 (2000) 171–185.
[4] C.-Y. Chen, M. Wang, J.-Y. Li, N. Pootrakulchote, L. Alibabaei, C.-H. Ngoc-le, J.-D. Decoppet, J.-H. Tsai, C. Grätzel, C.-G. Wu, S.M. Zakeeruddin, M. Grätzel, ACS Nano 3 (2009) 3103–3109.
[5] Y.-H. Lai, C.-W. Chiu, J.-G. Chen, C.-C. Wang, J.-J. Lin, K.-F. Lin, K.-C. Ho, Solar Energy Materials and Solar Cells 93 (2009) 1860–1864.
[6] M. Berginc, M. Hocevar, U. Opara Krasovec, A. Hinsch, R. Sastrawan, M. Topic, Thin Solid Films 516 (2008) 4645–4650.
[7] Y. Zhao, X. Sheng, J. Zhai, L. Jiang, C. Yang, Z. Sun, Y. Li, D. Zhu, ChemPhysChem 8 (2007) 856–861.
[8] Q.F. Zhang, T.R. Chou, B. Russo, S.A. Jenekhe, G.Z. Cao, Angewandte Chemie International Edition 47 (2008) 2402–2406.
[9] H.-M. Cheng, W.-F. Hsieh, Energy & Environmental Science 3 (2010) 442–447.
[10] M. Law, L.E. Greene, J.C. Johnson, R. Saykally, P.D. Yang, Nature Materials 4 (2005) 455–459.
[11] H.M. Cheng, W.H. Chiu, C.H. Lee, S.Y. Tsai, W.F. Hsieh, Journal of Physical Chemistry C 112 (2008) 16359–16364.
[12] Y. Dai, Y. Zhang, Q.K. Li, C.W. Nan, Chemical Physics Letters 358 (2002) 83–86.
[13] C.H. Lee, W.H. Chiu, K.M. Lee, W.H. Yen, H.F. Lin, W.F. Hsieh, J.M. Wu, Electrochimica Acta 55 (2010) 8422–8429.
[14] W.H. Chiu, C.H. Lee, H.M. Cheng, H.F. Lin, S.C. Liao, J.M. Wu, W.F. Hsieh, Energy & Environmental Science 2 (2009) 694–698.
[15] H.F. Lin, S.C. Liao, S.W. Hung, Journal of Photochemistry and Photobiology A: Chemistry 174 (2005) 82–87.
[16] T.S. Ko, S. Yang, H.C. Hsu, C.P. Chu, H.F. Lin, S.C. Liao, T.C. Lu, H.C. Kuo, W.F. Hsieh, S.C. Wang, Materials Science and Engineering: B 134 (2006) 54–58.
[17] S. Ito, T.N. Murakami, P. Comte, P. Liska, C. Grätzel, M.K. Nazeeruddin, M. Grätzel, Thin Solid Films 516 (2008) 4613–4619.
[18] T. Horiuchi, H. Miura, K. Sumioka, S. Uchida, Journal of the American Chemical Society 126 (2004) 12218–12219.
[19] S.Y. Huang, G. Schlichthorl, A.J. Nozik, M. Grätzel, A.J. Frank, The Journal of Physical Chemistry B 101 (1997) 2576–2582.
[20] W. Kubo, S. Kambe, S. Nakade, T. Kitamura, K. Hanabusa, Y. Wada, S. Yanagida, The Journal of Physical Chemistry B 107 (2003) 4374–4381.
[21] S. Ito, M. Grätzel, F. Fabregat-Santiago, I. Mora-Sero, J. Bisquert, T. Bessho, H. Imai, The Journal of Physical Chemistry B 110 (2006) 25210–25221.
[22] M. Adachi, M. Sakamoto, J. Jiu, Y. Ogata, S. Isoda, The Journal of Physical Chemistry B 110 (2006) 13872–13880.
[23] A.J. Bard, L.R. Faulkner, Electrochemical Methods: Fundamentals and Applications, Wiley, NY, 1980, p. 384.
[24] K.M. Lee, P.Y. Chen, C.P. Lee, K.C. Ho, Journal of Power Sources 190 (2009) 573–577.